Hole diffusion across leaky amorphous TiO_2 coating layers for catalytic water splitting at photoanodes

Zhendong Guo,* Francesco Ambrosio, and Alfredo Pasquarello

Chaire de Simulation à l'Echelle Atomique (CSEA), Ecole Polytechnique Fédérale de Lausanne (EPFL), CH-1015 Lausanne, Switzerland

E-mail: Zhendong.Guo@epfl.ch

Phone: +41 21 6933423. Fax: +41 21 693 5419

Abstract

We investigate the mechanism of hole diffusion across leaky amorphous TiO_2 (am-TiO_2) layers. Through *ab initio* molecular dynamics simulations, we construct an atomistic model of am-TiO_2 consistent with the experimental characterization. We first demonstrate that the oxygen vacancies do not occur in am-TiO_2, as they can be assimilated by the amorphous structure upon structural rearrangement. Hence, their role in hole diffusion is ruled out. In contrast, O-O peroxy linkages are formed in pristine am-TiO_2 upon injection of excess holes, with an associated defect level lying at 1.25 $\pm$ 0.15 eV above the valence band of the material. We show that such linkages can provide a viable mechanism for hole diffusion in am-TiO_2, as illustrated by a diffusion path of 1.2 nm with energy barriers lower than 0.5 eV in our atomistic model of am-TiO_2.

Titanium dioxide has been widely studied in the last decades due to its promising performance in a variety of novel technologies, such as dye-sensitized solar cells,[1] hydrogen storage,[2] photocatalytic water splitting,[3] and sensors.[4] In this context, most of the ongoing theoretical research has focussed mainly on crystalline phases of TiO_2, such as rutile, anatase, and brookite, with a particular focus on the electronic structure,[5–9] the surface chemistry,[10,11] and the TiO_2-water interface.[12–14] However, more recently amorphous TiO_2 (am-TiO_2) has attracted the interest of a growing scientific community, due to its possible application as switching material in resistive memory devices,[15] blocking layer in bulk heterojunction solar cells,[16] and surface passivation layer in biosensors.[17] A deep interest in the electronic properties of am-TiO_2 has arisen by recent unexpected observations[18,19] of the performance of this material as a coating layer for photoanodes in photocatalytic water splitting.[18,20–23] In particular, an am-TiO_2 overlayer has been used to stabilize Si, GaAs, GaP, and Fe_2O_3 photoanodes.[18,19] Surprisingly, the insulating overlayer of am-TiO_2 does not only protect the photocatalyst from degradation, but it also allows the photogenerated holes to diffuse through the amorphous and to reach the interface with liquid water, thus behaving as a leaky channel rather than as an insulating layer.[18] An attempt to explain this leaky

behavior in terms of oxygen vacancy hopping has recently been put forward,[24] while a possible role of extrinsic defects has been excluded due to the low estimated mobility of charge carriers.[25,26] However, the nature of intrinsic defects in amorphous materials has recently been questioned and it has been proposed that oxygen vacancies may actually not occur in amorphous oxides.[27] Therefore, it is of interest to investigate in more detail the possible transport mechanisms of holes in a technologically revelant material, such as am-TiO_2.

In this Communication, we combine electronic-structure calculations, molecular dynamics simulations (MD) and nudge elastic band (NEB) calculations to study the mechanism of hole diffusion across amorphous TiO_2 layers. We first build an atomistic model of am-TiO_2 of which the structural and electronic properties are consistent with available experiments. Next, we investigate the stability of the oxygen vacancy and find that structural rearrangements in the amorphous can assimilate oxygen vacancies, thus excluding them as a possible channel for hole diffusion across the material. At variance, we find that excess holes in the material lead to the formation of O-O peroxy linkages with a defect level at 1.25 $\pm$ 0.15 eV above the valence band. Considering that an O-O peroxy linkage can store two holes and that these holes are released when the O-O pair is broken, we propose an exchange mechanism for hole conduction in am-TiO_2, which is based on the simultaneous breaking and forming of O-O peroxy linkages that share one O atom. Through NEB calculations, we demonstrate a hopping path as long as 1.2 nm with barriers of 0.3-0.5 eV, thus indicating that hole diffusion through O-O peroxy linkages is viable in am-TiO_2.

All the calculations are carried out with the freely available `CP2K` suite of codes,[28] which is based on the use of atomic basis sets and of a plane-wave expansion for the electron density. Norm-conserving Goedecker-Teter-Hutter pseudopotentials[29,30] are used to account for core-valence interactions. We use a triple-ζ correlation-consistent polarized basis set (cc-pVTZ)[31] for O atoms, and the shorter range molecularly optimized double-zeta basis set with one polarization function (DZVP-MOLOPT-SR-GTH)[32] for Ti atoms. The plane-wave basis set is delimited by a kinetic-energy cutoff of 500 Ry. The sampling of the Brillouin zone

is achieved at the Γ point. Structural relaxations and molecular dynamics (MD) simulations are carried out with the Perdew, Burke, and Ernzerhof (PBE) functional,[33] which is shown to provide structural properties of crystalline rutile (r-TiO_2) and anatase (a-TiO_2) in good agreement with experiment (cf. Table 1 and Ref. 14).

MD simulations within the NVT ensemble are used to generate an atomistic model for am-TiO_2 through the melt-and-quench method. This technique has proved successful in generating atomistic models of amorphous oxides.[24,34–38] In these MD simulations, the temperature is controlled by a Nosé-Hoover thermostat.[39,40] A 3×3×4 supercell of rutile TiO_2 containing 216 atoms is taken as initial configuration. Through uniform elongation along the three Cartesian directions, the starting configuration is fixed at a density of ρ=3.82 g/cm^3, in order to stay within the experimental range (3.80-3.85 g/cm^3, Refs. 41 and 42). The prepared system undergoes molecular dynamics for a duration of 12 ps at a temperature of 4000 K, much higher than the melting point of TiO_2 (Ref. 43). This ensures that there is no memory from the initial crystalline structure upon MD. Then, we carry out a slow cooling procedure in which the temperature is decreased at a rate of 75 K/ps, until the final temperature of 300 K is reached. The lattice parameters of the model are then relaxed and we obtain a final structure with ρ =3.85 g/cm^3 (cf. Fig. 1), still consistent with the experimental range.[41,42] In the Supplementary Information,[44] we generated two additional models following the same protocol but with cooling rates of 300 and 600 K/ps. The structural and electronic properties of the generated models do not show any significant difference for the cooling rates investigated.

We test the structure of the achieved am-TiO_2 model by comparing the calculated radial distribution functions (RDF) with their experimental counterparts measured for sputtered amorphous TiO_2 layers (cf. Fig. 2).[45] The position of the main peaks and the shape of the curves for O-O, Ti-O, and Ti-Ti RDFs are in fair agreement with the experiment. In addition, we calculate the coordination number for oxygen and titanium atoms, considering a Ti-O cutoff distance of 2.4 Å, which corresponds to the position of the first minimum in

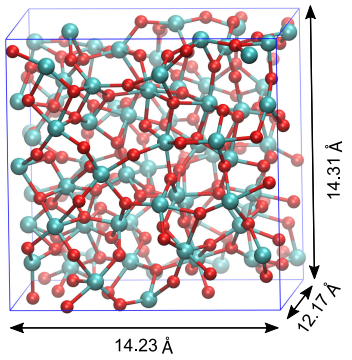

Figure 1: Atomistic representation of the am-TiO_2 model achieved in this work. The lattice parameters of the supercell are also reported. O atoms in red, Ti atoms in cyan.

the Ti-O RDF. We find that the majority of Ti atoms are sixfold coordinated (70%), but sevenfold (23%) and fivefold (7%) coordinations are also relevant. Threefold coordination is found to be prevalent for O atoms (80%), with only a small fraction of O atoms showing either twofold (14%) or fourfold (6%) coordination.

The electronic properties of am-TiO_2 are evaluated at the hybrid functional level, in order to overcome the band gap underestimation associated with semilocal functionals. In particular, we use the PBE0 functional,[46,47] in which we set the fraction of Fock exchange α to 0.15, as this value reproduces the experimental band gap of both r-TiO_2 and a-TiO_2 (cf. Table 1). We refer to this level of theory as to PBE0(α). Hybrid-functional calculations are performed using the auxiliary density matrix method,[47–49] available in `CP2K`. The am-TiO_2 model constructed in this work has a band gap of 3.42 eV, close to the experimental range (3.20-3.40 eV).[50–53]

In this work, we investigate charge transport through defect states. Extrinsic charge carriers are ruled out by their low mobilities.[25,26] Furthermore, the hopping through extrinsic impurities would require excessively high defect concentrations. Therefore, we focus in this study on intrinsic defects, such as vacancies and interstitials, which result from stoichiometric imbalance. For am-TiO_2, it sufficient to focus on oxygen related defects as the concentration imbalance due to missing or excess Ti atoms would lead to equivalent defects in the relaxed amorphous oxide.[27] Hence, the study of oxygen vacancies and interstitials is expected to give

Table 1: Calculated lattice parameters and mass density ρ at the PBE level for am-TiO_2, r-TiO_2, and a-TiO_2. The band gaps E_g are calculated at the PBE0 level with $\alpha = 0.15$, on structural configurations achieved at the PBE level. Results for r-TiO_2 and a-TiO_2 are taken from Ref. 14. Experimental values for both structural and electronic properties are reported for comparison.

	a (Å)	b (Å)	c (Å)	ρ (g/cm^3)	E_g (eV)
am-TiO_2					
Present theory	14.31	14.23	12.17	3.85	3.42
Expt.				3.80-3.85[a–d]	3.20-3.40[e,f]
r-TiO_2					
Present theory	4.66		3.00	4.07	3.02
Expt.	4.59		2.96	4.25	3.00[g]
a-TiO_2					
Present theory	3.81		9.67	3.79	3.35
Expt.	3.79		9.51	3.89	3.36[h,i]

[a] Ref. 50. [b] Ref. 51. [c] Ref. 52. [d] Ref. 53. [e] Ref. 41.

[f] Ref. 42. [g] Ref. 54. [h] Ref. 55. [i] Ref. 56.

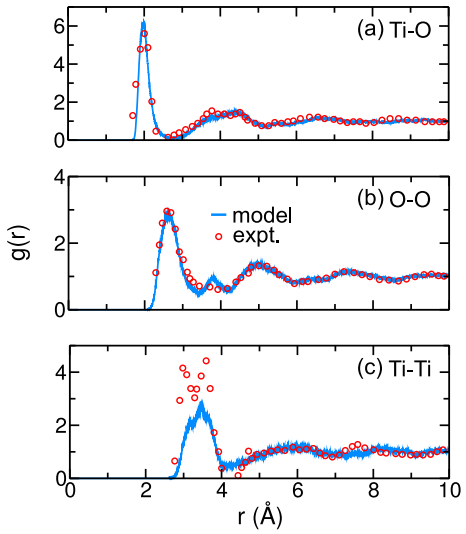

Figure 2: Radial distribution functions g(r) for (a) Ti-O, (b) O-O, and (c) Ti-Ti, as achieved from 3-ps-long molecular dynamics of the atomistic am-TiO_2 model at 300 K. RDFs as achieved from X-ray diffraction for sputtered TiO_2 amorphous layers[45] are shown for comparison.

a comprehensive account of the defects states relevant to charge transport.

First, we analyze the stability of the oxygen vacancy in am-TiO_2. We create an oxygen vacancy by removing a single O atom from the am-TiO_2 model and relax the structure of the neutral defect at the PBE level. This procedure is carried out for ten different oxygen atoms, which show variations in their local chemical environment. The electronic structure of the system is carried out at the hybrid functional level before and after the structural relaxation of the neutral vacancy. The wave function corresponding to the occupied defect state is always found to localize within the vacancy prior to relaxation [cf. Fig. 3(a)]. However, upon structural relaxation, the vacancy is completely assimilated by the amorphous structure in all the studied cases, and the associated wave function is found to be delocalized [cf. Fig. 3(b)]. This corresponds to a shift of the defect level towards the conduction band edge [cf. Fig. 3(c)]. Similar results are achieved for the +2 charge state. Overall, the removal of an O atom has produced a defect-free substoichiometric oxide, am-$TiO_{2-\delta}$, similarly to what has been observed previously for oxygen-deficient amorphous HfO_2 and amorphous Al_2O_3.[27,36] Hence, unlike for the crystalline phases of TiO_2, oxygen vacancies do not occur in the amorphous material. By consequence, the hopping of holes in am-TiO_2 through defect states associated with this kind of defect cannot be supported. Equivalent results are achieved when a Ti atom is removed from the atomistic model of am-TiO_2.

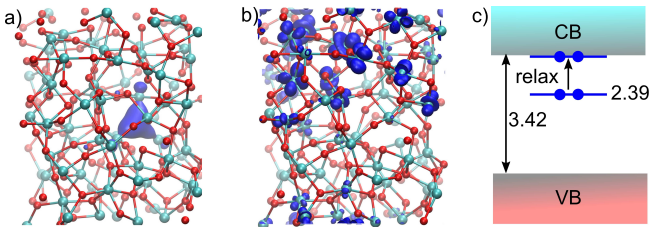

Figure 3: Isosurface representation (blue) of the wave function corresponding to the highest occupied single-particle energy level associated with the neutral oxygen vacancy (a) before and (b) after structural relaxation; O atoms in red, Ti atoms in cyan. (c) Evolution of the Kohn-Sham energy level associated with the defect state upon structural relaxation. Energies are given in eV and are referred to the VBM of pristine am-TiO_2.

Next, considering an oxygen interstitial is equivalent to introducing two extra holes,

as the oxygen atom only takes the -2 charge state.[27] Hence, we address the case of excess oxygen by adding two holes to the system and by carrying out MD simulations with the PBE functional. We use a temperature of 1000 K to accelerate the crossing of energy barriers. After 3 ps of simulation, the system has relaxed and its energy has undergone a decrease of ~ 2 eV. The stabilization results from the rearrangement of the amorphous structure leading to the formation of an O-O peroxy linkage with a bond length of 1.44 Å [cf. Fig. 4(a)]. To examine the stability of the O-O peroxy bond in am-TiO_2, we carry out MD simulations at a higher temperature of 1500 K for 5 ps and find that this feature is preserved. The O-O moiety is found to disappear upon injection of two electrons in the system. We repeat this computational procedure using 30 different starting configurations, as achieved from the MD of the uncharged am-TiO_2, and the O-O pair is systematically recovered. In particular, we can distinguish two bonding patterns for the peroxy linkage: (i) the two O atoms in the peroxy linkage form one bond to the same Ti atom [cf. Fig. 4(a)] and (ii) the O atoms are bonded to different Ti atoms [cf. Fig. 4(c)]. The former is generally found to be less stable than the latter by 0.2 eV, because of the significant distortion of the O-Ti-O angle. In our analysis, the bonding between O and Ti atom is assigned according to a Ti-O cutoff distance of 2.4 Å, which corresponds to the first minimum of the Ti-O radial distribution function [cf. Fig. 2(a)]. The O-O peroxy linkages are easily recognized as their average bond length (1.46 Å) is much lower than distances between second-neighbor O atoms, which exceed 2 Å, as can be inferred from the O-O RDF in Fig. 2(b).

We characterize the electronic levels of the observed defect using the grand-canonical formulation in which the defect formation $E_{\rm f}[X^q]$ is expressed as a function of the Fermi energy $\epsilon_{\rm F}$, defined with respect to the valence band maximum (VBM) $\epsilon_{\rm v}$ of the bulk system:[57,58]

$$\begin{aligned} E_{\rm f}[X^q] = \quad & E_{\rm tot}[X^q] + E^q_{\rm corr} - E_{\rm tot}[\text{bulk}] \\ & - \textstyle\sum_i n_i\mu_i + q[\epsilon_{\rm F} + \epsilon_{\rm v} + \Delta\upsilon_{0/\rm b}], \end{aligned} \tag{1}$$

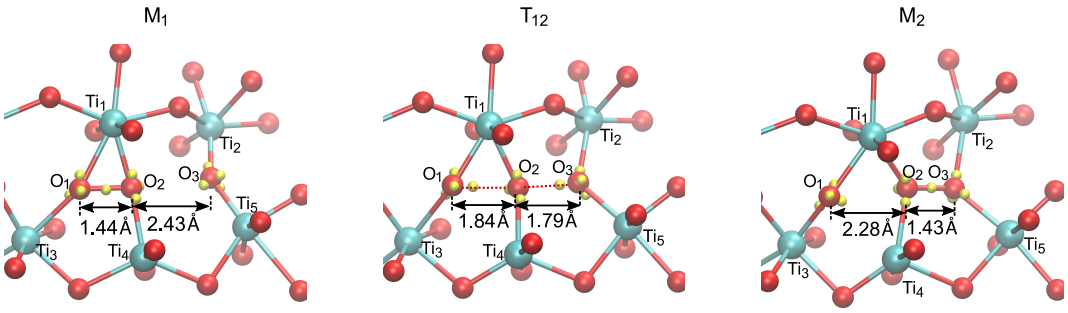

Figure 4: Representation of am-TiO_2 with an O-O peroxy linkage in a configuration in which the O atoms involved in the O-O bond (a) are linked to the same Ti atom or (c) are bonded to different Ti atoms. The structures in (a) and (c) correspond to local minima denoted M_1 and M_2 (cf. main text). In (b), we illustrate the transition state denoted T_{12}, which connects M_1 and M_2, as achieved from NEB calculations. The yellow spheres represent the centers of maximally localized Wannier functions associated with the relevant O atoms. The atoms denoted Ti_2, Ti_3, and Ti_5 are sixfold coordinated, whereas Ti_1 and Ti_4 are sevenfold and fivefold coordinated, respectively.

where $E_{\rm tot}[X^q]$ is the total energy of the supercell with a defect X in the charge state q, $E_{\rm tot}[\rm bulk]$ the total energy of bulk am-TiO_2, n_i the number of added or subtracted atoms of the species i needed to create the defect X, and μ_i the respective chemical potentials. The potential alignment term $\Delta v_{0/\rm b}$ accounts for the potential shift between the bulk and the neutral defect calculation.[58] $E^q_{\rm corr}$ is a finite-size electrostatic correction associated to the use of periodic supercells.[58,59] The charge transition level $\epsilon(q/q')$ is defined as the specific value of $\epsilon_{\rm F}$ for which the formation energies in the charge states q and q' coincide. From the 30 different structural models with two injected holes, we find an average $+2/0$ thermodynamic charge transition level of the peroxy linkage at 1.25 eV above the VBM, as illustrated in Fig. 5. The defect distribution is characterized by a standard deviation of 0.15 eV. The energy levels and the O-O bond lengths for the 30 structural models are given in the Supplementary Information.[44]

The distribution of calculated defect levels is reported in Fig. 5 with respect to the band alignments[18,60–62] between am-TiO_2 and the three semiconductors considered in the experiment of Ref. 18, namely Si, GaAs, and GaP. In this experiment, holes in the p-type semiconductor reach the catalytic surface by conduction through a thin layer of am-TiO_2 deposited

on the semiconductor.[18] The large currents observed in the experiment preclude conduction of holes through the valence band of am-TiO_2, which involves barriers corresponding to the valence band offsets, i.e. 2.22, 2.02, and 1.42 eV for Si, GaAs, and GaP, respectively (cf. Fig. 5).[18] We here suggest that the conduction occurs through charge hopping associated with the +2/0 level of the O-O defect. This conduction channel lowers the barrier for charge injection into am-TiO_2 by $\sim$ 1.25 eV for the three semiconductors, providing a rationale for the large currents observed in the experiment.[18]

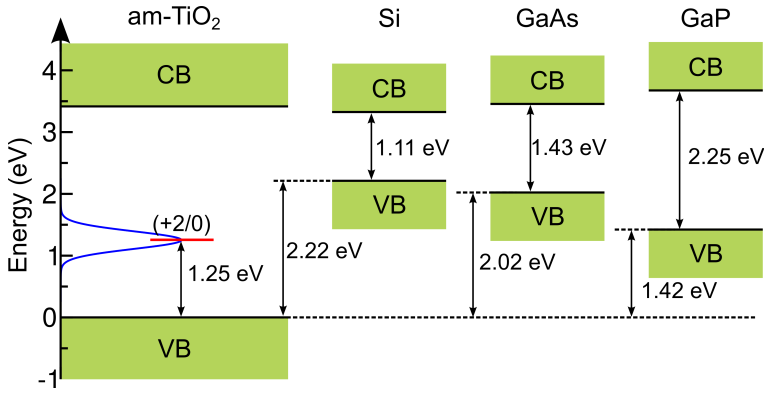

Figure 5: Energy diagram illustrating the distribution of +2/0 charge transition levels associated with O-O defects in am-TiO_2. The band edges of Si, GaAs, and GaP are aligned with those of am-TiO_2 using the measured results of Refs. 18,60–62. All energies are given in eV and referred to the VBM of the pristine am-TiO_2 model.

To reveal the hole transport mechanism through O-O peroxy linkages upon injection in am-TiO_2, we investigate the breaking of an O-O pair followed by its simultaneous formation in a neighbouring location. We first consider a mechanism in which the initial and final O-O peroxy linkages do not share a common O atom. We add two extra holes and observe the formation of a second O-O pair within the same model at a distance of $\sim$4 Å from the initial O-O pair. We then construct initial and final configurations in the +2 charge state, both of which contain a single O-O pair, but in different locations. To determine the transition barrier, we perform NEB calculations at the PBE level with the improved tangent (IT) method,[63] considering nine replicas between the initial and final configurations. In this way, we obtain a transition barrier of 1.0 eV resulting from the high energy cost for breaking the

O-O bond at the transition state.

We then investigate a second transport mechanism, in which the O-O peroxy linkages of the initial and final states share an O atom. This mechanism relies on the fact that all oxygen atoms can be involved in the formation of at least two different O-O pairs by relatively minor structural adjustments. The oxygen atoms do not diffuse across the material and they recover their original positions once the positive charge has passed. In this case, we have been able to construct a minimum energy path involving four subsequent steps by which the charge associated with an O-O pair diffuses over a distance of 1.2 nm, with barriers ranging between 0.3 and 0.5 eV (cf. Fig. 6). The lower barriers found in this second mechanism can be explained by analyzing the structure of the transition states T_{ij} between two consecutive energy minima M_i and M_j. In fact, in the transition state T_{ij}, the O atom which is shared by the initial and final O-O pairs is found to be almost equidistant from the O atoms involved in the O-O linkages in M_i and M_j [cf. Fig. 4(b)], with average bond lengths of about 1.8 Å, longer by 0.36 Å than those observed in an isolated peroxy bond. Hence, the diffusion proceeds without ever completely breaking the O-O bond and the transition barriers are lower. This behavior can further be illustrated in terms of maximally localized Wannier functions,[64] which give a real-space representation of the electron localization. In Fig. 4, we show the evolution of the centers of such Wannier functions for the relevant O atoms as the hopping proceeds. In the initial state, the Wannier center representing the O_1-O_2 bond is located centrally, but moves closer to O_1 in the transition state, where O_2 attracts one of the lone pairs of O_3, in view of forming a regular O_2-O_3 bond in the final state. This process gives a diffusion mechanism by which the holes leak through the am-TiO_2 layer, despite the presence of a well defined band gap that supports its insulating character. The energy barriers are found to be only marginally affected by the density functional as IT-NEB calculations at the PBE0(α) level are found to give differences smaller than 0.07 eV.

It should be noted that the energy barriers calculated in this work may represent an upper-bound limit. In fact, given the disordered environment and the possibility of forming

O-O pairs anywhere in the oxide, the diffusion is expected to proceed through percolation, generally resulting in overall lower transition barriers than the ones encountered in the present study. Furthermore, the barrier is related to the distance between O atoms, which in turn depends on the concentration of oxygen in the material. Therefore, lower barriers are expected to occur in oxygen-rich conditions or in amorphous layers of higher density.

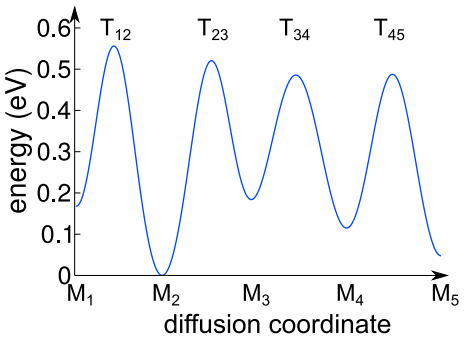

Figure 6: (a) Energy diagram illustrating the hole diffusion through O-O peroxy linkages in am-TiO_2 along a diffusion coordinate visiting several minima M_i in sequence ($i = 1, 2, ...5$). Transition states T_{ij} connect sequential minima M_i and M_j, where $j = i + 1$. The minima M_1 and M_5 are separated by a distance of 1.2 nm.

In conclusion, we studied hole diffusion across amorphous TiO_2 layers through O-O peroxy linkages. We generated a model for amorphous TiO_2 through *ab initio* molecular dynamics simulations, and found good agreement with the experimental characterization. Then, we demonstrated that oxygen vacancies cannot contribute to hole transport, as these intrinsic defects do not occur in am-TiO_2. In contrast, O-O peroxy linkages are formed in pristine am-TiO_2 upon injection of excess holes, and give a defect distribution centered at 1.25 eV above the valence band. The hole diffusion in am-TiO_2 through an exchange mechanism involving such O-O pairs is viable and proceeds with energy barriers lower than 0.5 eV.

Acknowledgement

This work has been performed in the context of the National Center of Competence in Research (NCCR): Materials' Revolution: Computational Design and Discovery of Novel Materials (MARVEL) of the Swiss National Science Foundation. We used computational

resources of the Swiss National Supercomputing Center (CSCS) and of the Scientific IT Application Support (SCITAS) of EPFL.

References

(1) O'Regan, B.; Grätzel, M. A low-cost, high-efficiency solar cell based on dye-sensitized colloidal TiO_2 films. *Nature* **1991**, *353*, 737.

(2) Bavykin, D. V.; Lapkin, A. A.; Plucinski, P. K.; Friedrich, J. M.; Walsh, F. C. Reversible Storage of Molecular Hydrogen by Sorption into Multilayered TiO_2 Nanotubes. *J. Phys. Chem. B* **2005**, *109*, 19422–19427.

(3) Fujishima, A.; Honda, K. Electrochemical photolysis of water at a semiconductor electrode. *Nature* **1972**, *238*, 37.

(4) Garzella, C.; Comini, E.; Tempesti, E.; Frigeri, C.; Sberveglieri, G. TiO_2 thin films by a novel sol-gel processing for gas sensor applications. *Sens. Actuators B* **2000**, *68*, 189–196.

(5) Morgan, B. J.; Watson, G. W. Polaronic trapping of electrons and holes by native defects in anatase TiO_2. *Phys. Rev. B* **2009**, *80*, 233102.

(6) Landmann, M.; Rauls, E.; Schmidt, W. G. The electronic structure and optical response of rutile, anatase and brookite TiO_2. *J. Phys.: Condens. Matter* **2012**, *24*, 195503.

(7) Di Valentin, C.; Pacchioni, G.; Selloni, A. Origin of the different photoactivity of N-doped anatase and rutile TiO_2. *Phys. Rev. B* **2004**, *70*, 085116.

(8) Morgan, B. J.; Watson, G. W. Intrinsic n-type Defect Formation in TiO_2: A Comparison of Rutile and Anatase from GGA+U Calculations. *J. Phys. Chem. C* **2010**, *114*, 2321–2328.

(9) Deskins, N. A.; Rousseau, R.; Dupuis, M. Localized Electronic States from Surface Hydroxyls and Polarons in TiO_2(110). *J. Phys. Chem. C* **2009**, *113*, 14583–14586.

(10) Ambrosio, F.; Martsinovich, N.; Troisi, A. What is the best anchoring group for a dye in a dye-sensitized solar cell? *J. Phys. Chem. Lett.* **2012**, *3*, 1531–1535.

(11) Ip, C. M.; Troisi, A. A computational study of the competing reaction mechanisms of the photo-catalytic reduction of CO_2 on anatase(101). *Phys. Chem. Chem. Phys.* **2016**, *18*, 25010–25021.

(12) Cheng, J.; Sprik, M. Acidity of the aqueous rutile TiO_2 (110) surface from density functional theory based molecular dynamics. *J. Chem. Theory Comput.* **2010**, *6*, 880–889.

(13) Hussain, H.; Tocci, G.; Woolcot, T.; Torrelles, X.; Pang, C.; Humphrey, D.; Yim, C.; Grinter, D.; Cabailh, G.; Bikondoa, O. et al. Structure of a model TiO_2 photocatalytic interface. *Nat. Mater.* **2017**, *16*, 461.

(14) Guo, Z.; Ambrosio, F.; Chen, W.; Gono, P.; Pasquarello, A. Alignment of redox levels at semiconductor-water interfaces. *Chem. Mater.* **2018**, *30*, 94–111.

(15) Jeong, H. Y.; Lee, J. Y.; Choi, S.-Y. Interface-Engineered Amorphous TiO_2-Based Resistive Memory Devices. *Adv. Funct. Mater.* **2010**, *20*, 3912–3917.

(16) Muñoz-Rojas, D.; Sun, H.; Iza, D. C.; Weickert, J.; Chen, L.; Wang, H.; Schmidt-Mende, L.; MacManus-Driscoll, J. L. High-speed atmospheric atomic layer deposition of ultra thin amorphous TiO_2 blocking layers at 100^o C for inverted bulk heterojunction solar cells. *Prog. Photovoltaics* **2013**, *21*, 393–400.

(17) Ozasa, K.; Nemoto, S.; Hara, M.; Maeda, M.; Mochitate, K. The passivation/modification of AlGaAs/GaAs surfaces by amorphous TiO_2 for the bio-sensing use in electrolytes. *Surf. Sci.* **2007**, *601*, 4536–4540.

(18) Hu, S.; Shaner, M. R.; Beardslee, J. A.; Lichterman, M.; Brunschwig, B. S.; Lewis, N. S. Amorphous TiO_2 coatings stabilize Si, GaAs, and GaP photoanodes for efficient water oxidation. *Science* **2014**, *344*, 1005–1009.

(19) Ahmed, M. G.; Kretschmer, I. E.; Kandiel, T. A.; Ahmed, A. Y.; Rashwan, F. A.; Bahnemann, D. W. A facile surface passivation of hematite photoanodes with TiO_2 overlayers for efficient solar water splitting. *ACS Appl. Mater. Interfaces* **2015**, *7*, 24053–24062.

(20) Niu, W.; Li, X.; Karuturi, S. K.; Fam, D. W.; Fan, H.; Shrestha, S.; Wong, L. H.; Tok, A. I. Y. Applications of atomic layer deposition in solar cells. *Nanotechnology* **2015**, *26*, 064001.

(21) McDowell, M. T.; Lichterman, M. F.; Carim, A. I.; Liu, R.; Hu, S.; Brunschwig, B. S.; Lewis, N. S. The influence of structure and processing on the behavior of TiO_2 protective layers for stabilization of n-Si/TiO_2/Ni photoanodes for water oxidation. *ACS Appl. Mater. Interfaces* **2015**, *7*, 15189–15199.

(22) Gu, J.; Yan, Y.; Young, J. L.; Steirer, K. X.; Neale, N. R.; Turner, J. A. Water reduction by a p-$GaInP_2$ photoelectrode stabilized by an amorphous TiO_2 coating and a molecular cobalt catalyst. *Nat. Mater.* **2016**, *15*, 456.

(23) Bronneberg, A. C.; Höhn, C.; van de Krol, R. Probing the interfacial chemistry of ultrathin ALD-grown TiO_2 films: an in-line XPS study. *J. Phys. Chem. C* **2017**, *121*, 5531–5538.

(24) Pham, H. H.; Wang, L.-W. Oxygen vacancy and hole conduction in amorphous TiO_2. *Phys. Chem. Chem. Phys.* **2015**, *17*, 541–550.

(25) Pham, H. H.; Wang, L.-W. Electronic structures and current conductivities of B, C, N and F defects in amorphous titanium dioxide. *Phys. Chem. Chem. Phys.* **2015**, *17*, 11908–11913.

(26) Ghuman, K. K.; Singh, C. V. Self-Trapped Charge Carriers in Defected Amorphous TiO_2. *J. Phys. Chem. C* **2016**, *120*, 27910–27916.

(27) Guo, Z.; Ambrosio, F.; Pasquarello, A. Oxygen defects in amorphous Al_2O_3: A hybrid functional study. *Appl. Phys. Lett.* **2016**, *109*, 062903.

(28) VandeVondele, J.; Krack, M.; Mohamed, F.; Parrinello, M.; Chassaing, T.; Hutter, J. Quickstep: Fast and accurate density functional calculations using a mixed Gaussian and plane waves approach. *Comput. Phys. Commun.* **2005**, *167*, 103–128.

(29) Goedecker, S.; Teter, M.; Hutter, J. Separable dual-space Gaussian pseudopotentials. *Phys. Rev. B* **1996**, *54*, 1703–1710.

(30) Hartwigsen, C.; Goedecker, S.; Hutter, J. Relativistic separable dual-space Gaussian pseudopotentials from H to Rn. *Phys. Rev. B* **1998**, *58*, 3641–3662.

(31) Dunning, T. H. Gaussian basis sets for use in correlated molecular calculations. I. The atoms boron through neon and hydrogen. *J. Chem. Phys.* **1989**, *90*, 1007–1023.

(32) VandeVondele, J.; Hutter, J. Gaussian basis sets for accurate calculations on molecular systems in gas and condensed phases. *J. Chem. Phys.* **2007**, *127*, 114105.

(33) Perdew, J. P.; Burke, K.; Ernzerhof, M. Generalized Gradient Approximation Made Simple. *Phys. Rev. Lett.* **1996**, *77*, 3865–3868.

(34) Sarnthein, J.; Pasquarello, A.; Car, R. Model of vitreous SiO_2 generated by an ab initio molecular-dynamics quench from the melt. *Phys. Rev. B* **1995**, *52*, 12690–12695.

(35) Umari, P.; Pasquarello, A. Fraction of Boroxol Rings in Vitreous Boron Oxide from a First-Principles Analysis of Raman and NMR Spectra. *Phys. Rev. Lett.* **2005**, *95*, 137401.

(36) Broqvist, P.; Pasquarello, A. First principles investigation of defects at interfaces between silicon and amorphous high-κ oxides. *Microelectron. Eng.* **2007**, *84*, 2022–2027.

(37) Broqvist, P.; Binder, J. F.; Pasquarello, A. Band offsets at the Ge/GeO_2 interface through hybrid density functionals. *Appl. Phys. Lett.* **2009**, *94*, 141911.

(38) Colleoni, D.; Miceli, G.; Pasquarello, A. Band alignment and chemical bonding at the $GaAs/Al_2O_3$ interface: A hybrid functional study. *Appl. Phys. Lett.* **2015**, *107*, 211601.

(39) Nosé, S. A unified formulation of the constant temperature molecular dynamics methods. *J. Chem. Phys.* **1984**, *81*, 511–519.

(40) Hoover, W. G. Canonical dynamics: Equilibrium phase-space distributions. *Phys. Rev. A* **1985**, *31*, 1695–1697.

(41) Mergel, D.; Buschendorf, D.; Eggert, S.; Grammes, R.; Samset, B. Density and refractive index of TiO_2 films prepared by reactive evaporation. *Thin Solid Films* **2000**, *371*, 218–224.

(42) Saleem, M. R.; Honkanen, S.; Turunen, J. Thermal properties of TiO_2 films fabricated by atomic layer deposition. *IOP Conf. Ser. Mater. Sci. Eng.* **2014**, *60*, 012008.

(43) Brauer, G.; Littke, W. Über den schmelzpunkt und die thermische Dissoziation von Titandioxyd. *J. Inorg. Nucl. Chem.* **1960**, *16*, 67–76.

(44) The Supplementary Information contains a detailed comparison of the structural and electronic properties of am-TiO_2 models produced through the melt-and-quench method with different cooling rates and a description of 30 O-O peroxy linkage models in terms of their charge transition levels and bond lengths.

(45) Petkov, V.; Holzhüter, G.; Tröge, U.; Gerber, T.; Himmel, B. Atomic-scale structure of amorphous TiO_2 by electron, X-ray diffraction and reverse Monte Carlo simulations. *J. Non-Cryst. Solids* **1998**, *231*, 17–30.

(46) Adamo, C.; Barone, V. Toward reliable density functional methods without adjustable parameters: The PBE0 model. *J. Chem. Phys.* **1999**, *110*, 6158–6170.

(47) Guidon, M.; Hutter, J.; VandeVondele, J. Robust Periodic Hartree-Fock Exchange for Large-Scale Simulations Using Gaussian Basis Sets. *J. Chem. Theory Comput.* **2009**, *5*, 3010–3021.

(48) Guidon, M.; Schiffmann, F.; Hutter, J.; VandeVondele, J. Ab initio molecular dynamics using hybrid density functionals. *J. Chem. Phys.* **2008**, *128*, 214104.

(49) Guidon, M.; Hutter, J.; VandeVondele, J. Auxiliary Density Matrix Methods for Hartree-Fock Exchange Calculations. *J. Chem. Theory Comput.* **2010**, *6*, 2348–2364.

(50) Amor, S.; Guedri, L.; Baud, G.; Jacquet, M.; Ghedira, M. Influence of the temperature on the properties of sputtered titanium oxide films. *Mater. Chem. Phys.* **2003**, *77*, 903–911.

(51) Takikawa, H.; Matsui, T.; Sakakibara, T.; Bendavid, A.; Martin, P. J. Properties of titanium oxide film prepared by reactive cathodic vacuum arc deposition. *Thin Solid Films* **1999**, *348*, 145–151.

(52) Zhao, Z.; Tay, B.; Lau, S.; Yu, G. Optical properties of titania films prepared by off-plane filtered cathodic vacuum arc. *J. Cryst. Growth* **2004**, *268*, 543–546.

(53) Zhang, M.; Lin, G.; Dong, C.; Wen, L. Amorphous TiO_2 films with high refractive index deposited by pulsed bias arc ion plating. *Surf. Coat. Technol.* **2007**, *201*, 7252–7258.

(54) Tang, H.; Prasad, K.; Sanjines, R.; Schmid, P.; Lévy, F. Electrical and optical properties of TiO_2 anatase thin films. *J. Appl. Phys.* **1994**, *75*, 2042–2047.

(55) Tang, H.; Berger, H.; Schmid, P.; Lévy, F.; Burri, G. Photoluminescence in TiO_2 anatase single crystals. *Solid State Commun.* **1993**, *87*, 847–850.

(56) Baldini, E.; Chiodo, L.; Dominguez, A.; Palummo, M.; Moser, S.; Yazdi-Rizi, M.; Auböck, G.; Mallett, B.; Berger, H.; Magrez, A. et al. Strongly bound excitons in anatase TiO_2 single crystals and nanoparticles. *Nat. Commun.* **2017**, *8*, 13.

(57) Alkauskas, A.; Broqvist, P.; Pasquarello, A. Defect levels through hybrid density functionals: Insights and applications. *Phys. Status Solidi B* **2011**, *248*, 775–789.

(58) Komsa, H.-P.; Rantala, T. T.; Pasquarello, A. Finite-size supercell correction schemes for charged defect calculations. *Phys. Rev. B* **2012**, *86*, 045112.

(59) Freysoldt, C.; Neugebauer, J.; Van de Walle, C. G. Fully *Ab Initio* Finite-Size Corrections for Charged-Defect Supercell Calculations. *Phys. Rev. Lett.* **2009**, *102*, 016402.

(60) Perfetti, P.; Patella, F.; Sette, F.; Quaresima, C.; Capasso, C.; Savoia, A.; Margaritondo, G. Experimental study of the GaP-Si interface. *Phys. Rev. B* **1984**, *30*, 4533–4539.

(61) Dahmen, M.; Rau, U.; Kawanaka, M.; Sone, J.; Werner, J. Band offset variations at Ge/GaAs (100) interfaces. *Appl. Phys. Lett.* **1993**, *62*, 261–263.

(62) Jain, N.; Zhu, Y.; Maurya, D.; Varghese, R.; Priya, S.; Hudait, M. K. Interfacial band alignment and structural properties of nanoscale TiO_2 thin films for integration with epitaxial crystallographic oriented germanium. *J. Appl. Phys.* **2014**, *115*, 024303.

(63) Henkelman, G.; Jónsson, H. Improved tangent estimate in the nudged elastic band method for finding minimum energy paths and saddle points. *J. Chem. Phys.* **2000**, *113*, 9978–9985.

(64) Marzari, N.; Mostofi, A. A.; Yates, J. R.; Souza, I.; Vanderbilt, D. Maximally localized Wannier functions: Theory and applications. *Rev. Mod. Phys.* **2012**, *84*, 1419–1475.

Graphical TOC Entry